LATVIAN JOURNAL OF PHYSICS AND TECHNICAL SCIENCES
2008, N 4
10.2478/v10047-008-0018-2

NUMERICAL SIMULATION OF CHARGE TRANSFER IN SHOCKED SILICON AT LOW PRESSURE

B. Martuzans, Yu. Skryl

Institute of Mathematics and Computer Science, University of Latvia,
29 Raiņa Blvd., Rīga, LV-1459, LATVIA

A numerical method for simulation of electron and hole diffusion in silicon in the temperature gradient created by the shock load is developed. To analyze the transfer process, a complete system of electro-thermo-diffusion equations for charge carriers was solved based on the Poisson equation. The numerical solution was obtained using the difference methods developed for semiconductor devices. The comparison of the experimental results with the numerical calculation shows a good correlation, which means that the thermo-diffusion of charge carriers in the shock wave front is the main factor responsible for polarization in the shocked silicon.

1. INTRODUCTION

Studies of electromotive forces (EMFs) induced by shock waves – the shock-induced polarization as a more widespread term – in condensed matter have quite a long history owing to a fundamental interest in the behaviour of materials under extreme conditions and the technological applications. It was first discovered that deformation of ionic crystals results in the appearance of electric potential between the deformed surfaces [1]. Later, the so-called impact EMF was observed in linear and nonlinear dielectrics [2, 3], semiconductors [4], and metals [5] under the shock load.

Physics of shock or impact EMF is complex and multifaceted. It has mostly been developed for dielectrics (see an excellent review by Mineev and Inanov [6]). Phenomenological models often used in earlier works (see, e.g. [7–9]) assume polarization of dielectric in the front of a plane shock wave. Advantages and disadvantages of this approach are discussed in great detail in review [6]. The explanation of shock-induced EMF is not that simple for semiconductors. Attempts to describe EMF with polarization mechanisms alone have failed. Many authors conclude that, along with polarization, there are other mechanisms – such as formation and migration of Frenkel's pair type point defects [4]. The situation is even more complex for metals, because the polarization models used for dielectrics do not work here at all. Therefore, other dynamic models were suggested, e.g., the diffusion of charge carriers from the wave front [10] and the increasing number of carriers at lattice deformations [11].

The present paper presents an attempt to estimate straightforward (numerically) the electric current created by a shock wave in the electrically-neutral silicon. It is supposed that the charge carriers and the ionized impurity can be separated owing to a temperature gradient of the shock wave front under some shock heating condition, thus creating a double electric layer. At the presence of some

conductivity this double layer can generate a nonzero electric current in an originally neutral sample of the semiconductor. It has been shown that the shock heating is sufficient for explanation of the experimental values of current in shocked silicon reported in [4]. Moreover, modelling of the conductivity change in the compression region has allowed also explanation of the time dependence of these currents [4] during propagation of the shock wave front through the sample.

We have developed a method for calculation of the drift-thermo-diffusion of electrons and holes, which makes it possible to obtain the magnitudes of voltages, electric field and currents in shocked semiconductors. In this study, general methods worked out for semiconductor devices [12, 13] were applied for simulation of the electric current induced by a temperature gradient in the shock wave front. Since many efficient numerical schemes are well known in this field, some success could have been expected. It turned out, however, that the problem of calculating the shock-induced currents is very complicated, and its solution is possible if the discrepancy of the electric potential in the modelled structure is small enough. The mentioned methods work quickly only in the regions of small concentrations of charge carriers, but when the concentration increases the number of iterations for obtaining the necessary precision also grows. Therefore, it is necessary to use high-speed computation tools (like the GRID-technology [14]) if these methods are to be applied to highly-doped semiconductors and metals. In the meantime, the most interesting problem is the determination of currents in metallic samples, since there is no clear picture in the interpretation of the large EMF in shocked metals.

2. SIMULATION OF SHOCK WAVES IN SILICON

All the necessary parameters of a shock wave can generally be derived for solids from the conservation laws in the same manner as for gases and liquids [15]. The difference is in the equation of state and in the equations of impulse and energy, where a stress component (or the material strength), σ_s, appears. This component describes solids, and its form depends on a specific model of the chosen solid. In particular, the elastic-plastic model is often used to simulate shock/impact waves [16, 17]. In this study, we will restrict ourselves to the elastic model. The complete elastic-plastic rheologic model for a specific material at high pressure is the subject of special discussion and is not treated here.

For the impact wave front the conservation laws of mass, impulse, and energy are valid. We will write these equations for the one-dimensional problem in Euler's coordinates [18]:

$$\frac{\partial \rho}{\partial t} + \frac{\partial (v\rho)}{\partial x} = 0 ; \tag{1}$$

$$\frac{\partial (\rho v)}{\partial t} + \frac{\partial (\rho v^2)}{\partial x} = \frac{\partial \sigma}{\partial x} ; \tag{2}$$

$$\frac{\partial}{\partial t}\left(\rho e + \frac{1}{2}\rho v^2 \right) + \frac{\partial}{\partial x}\left(\rho e v + \frac{1}{2}\rho v^3 \right) = \frac{\partial (\sigma v)}{\partial x} , \tag{3}$$

where ρ is the density;
v is the velocity;

e is the internal energy;
σ is Cauchy's stress;
x is the spatial coordinate;
t is the time.

To Eqs. (1–3) the well-known relation between the strain rate, $\dot{\varepsilon}$, and the velocity, v, for solid states [15] should be added:

$$\dot{\varepsilon} = \frac{\partial v}{\partial x}. \tag{4}$$

The Cauchy stress is

$$\sigma = \sigma_s + \sigma_v - p, \tag{5}$$

where p is the hydrostatic pressure. The material strength σ_s and the viscous stress σ_v can be presented in the following form [19]:

$$\sigma_s = 2G\dot{\varepsilon}; \tag{6}$$

$$\sigma_v = 2\nu\dot{\varepsilon}. \tag{7}$$

where G is the shear modulus and ν is the shear viscosity.

The equation of state (EOS) for the pressure as a function of the density and internal energy has been determined for the crystal as [20]

$$p = \rho_0 C^2 \mu \frac{1 - 0.5\gamma_0 \mu}{1 - S\mu} + \gamma_0 \rho_0 e, \tag{8}$$

$$\mu = 1 - \frac{\rho_0}{\rho}, \tag{9}$$

where ρ_0 is the initial density;
C is the longitudinal speed of sound under ambient conditions;
γ_0 is Gruneisen's coefficient;
S is some EOS parameter.

If the equation of state (8) is substituted into the conservation law equations (1–3), the following equations for the stationary shock wave could be obtained [21]:

$$\rho_0 C^2 \mu_1 \frac{1 - 0.5\gamma_0 \mu_1}{1 - S\mu_1} + \gamma_0 G \mu_1^2 = p_1 \left(1 - \frac{1}{2}\gamma_0 \mu_1\right), \tag{10}$$

$$v_1 = \mu_1 D, \tag{11}$$

$$\rho_0 D^2 = \frac{1}{2}\gamma_0 p_1 + \rho_0 C^2 \frac{1 - 0.5\gamma_0 \mu_1}{1 - S\mu_1} + 2G\left(1 + \frac{1}{2}\gamma_0 \mu_1\right), \tag{12}$$

$$p_1 = \rho_0 v_1 D - 2G\mu_1, \tag{13}$$

where D is the shock wave velocity,
p_1, v_1, μ_1 are the pressure, velocity and compression degree behind the shock front.

From Eq. (10) (or Hugoniot's equation) it is possible to define the maximum compression μ_1 in the shock wave if its amplitude p_1 is known. After that, from Eqs. (11, 12) the mass and shock wave velocities could be found. The additional equation (13) shows the relation between the found parameters.

It is very simple to define the parameters for a plastic wave. If $G = 0$, from Eqs. (10–12) we will have:

$$\mu_1 = \frac{\widetilde{p}_1}{1 + S\,\widetilde{p}_1}, \tag{14}$$

$$D = C\sqrt{1 + S\,\widetilde{p}_1}\,, \tag{15}$$

$$v_1 = C\,\frac{\widetilde{p}_1}{\sqrt{1 + S\,\widetilde{p}_1}}, \tag{16}$$

where $\widetilde{p}_1 = p_1 \big/ \rho_0 C^2$.

Also, for the plastic wave it is easy to obtain the important relation $D(v_1)$, which usually is defined experimentally. Using any of Eqs. (14–16) and Eq. (13) we obtain:

$$D = \frac{1}{2} C\left(\sqrt{S^2\widetilde{v}_1^{\,2} + 4} + S\widetilde{v}_1\right), \tag{17}$$

where $\widetilde{v}_1 = v_1 / C$.

Equation (17) somewhat differs from the well-known form: $D = D_0 + Sv_1$, where D_0 is a constant. The mentioned equation transforms into this form at large values of v_1 when D_0 asymptotically tends to zero. However, as is shown below, Eq. (17) describes the plastic wave much better (at least for silicon).

To obtain the dependences of wave parameters on the pressure for an elastic wave is not so trivial problem as for a plastic wave. An appropriate cubic equation should be solved not only for $D(v_1)$ but also for $\mu_1(p_1)$ if $G \neq 0$. However, the problem can be simplified at least for $\mu_1(p_1)$, since for an elastic wave $\mu_1 << 1$, so in this case the following quadratic equation can be solved:

$$\mu_1 = \frac{1}{\gamma_0\left(1 + S\widetilde{p}_1 - 2\widetilde{G}\right)} \cdot \left[1 + (S + \frac{1}{2}\gamma_0)\,\widetilde{p}_1 - \sqrt{4\widetilde{G}\gamma_0\widetilde{p}_1 + \left[1 + (S - \frac{1}{2}\gamma_0)\,\widetilde{p}_1\right]^2}\,\right], \tag{18}$$

where $\widetilde{G} = G \big/ \rho_0 C^2$.

Equation (18) transforms into Eq. (14) if $G = 0$. This is an advantage of the quadratic approach. It is impossible to obtain this transform if a linear approach is used for solving Eq. (10). A cubic equation can also be obtained from Eqs. (10–13): for $D(v_1)$ the dependence for the elastic wave is

$$\widetilde{D}^3 - a\widetilde{D}^2 + b\widetilde{D} + c = 0\,; \tag{19}$$

where

$$a = (S + \frac{1}{2}\gamma_0)\widetilde{v}_1\,,$$

$$b = \frac{1}{2}\gamma_0 S\widetilde{v}_1^2 - 2\widetilde{G} - 1\,,$$

$$c = (2\widetilde{G}S + \frac{1}{2}\gamma_0)\widetilde{v}_1\,,$$

which cannot be simplified because the condition $\widetilde{D} = D/C > 1$ is always valid. It is the easiest to express the solution of Eq. (19) in the trigonometric form:

$$\widetilde{D} = \frac{2}{3}\sqrt{a^2 - 3b}\cos\left[\frac{1}{3}\arcsin\left(\frac{2a^3 - 9ab - 27c}{2\sqrt{\left(a^2 - 3b\right)^3}}\right) - \frac{\pi}{6}\right] + \frac{a}{3}\,. \tag{20}$$

3. THE MODEL OF ELECTRON-HOLE TRANSFER IN SHOCKED SILICON

The shock-induced polarization of silicon, which presumably appears as a result of diffusive separation of electron-donor or hole-acceptor systems in the impurity-doped silicon under shock load, may be considered in much the same way as the process of ion separation in multicomponent plasmas [22]. The main reasons for the separation, in accordance with Zeldovich, are the differences in the diffusion coefficients in the shock front whose parameters – such as density, pressure and temperature – strongly vary. All of these parameters can make a certain contribution to the separation process. In the present model, the temperature gradient is considered as the main factor of the separation.

The method for calculation of the shock-induced polarization in silicon proposed here is based on the well-established numerical methods developed earlier for the electric characteristics of semiconductor devices [12, 13]. We will consider the basic equations for the electro-diffusive motion of charge carriers in shocked silicon taking into account the thermo-diffusion effects. Using the procedures developed by the authors of [23, 24], the complete system of drift-diffusion equations with the thermo-diffusion component can be written as

$$J_i = -D_i\left(\frac{\partial C_i}{\partial x} + \frac{z_i q C_i}{k_B T}\frac{\partial \varphi}{\partial x} + \frac{\alpha_{Ti} C_i}{T}\frac{\partial T}{\partial x}\right); \tag{21}$$

$$\frac{\partial C_i}{\partial t} = -\frac{\partial J_i}{\partial x}\,; \tag{22}$$

$$\frac{\partial}{\partial x}\left(\varepsilon\frac{\partial \varphi}{\partial x}\right) = -\frac{q}{\varepsilon_0}\sum_{i=1}^{N} z_i C_i\,, \tag{23}$$

where z_i is the charge number of a charge currier of species i (electrons or holes as donors or acceptors);
q is the electronic charge;
D_i is the diffusion coefficient;
C_i is the concentration of charge curriers;
φ is the electrostatic potential;
ε, ε_0 are the dielectric constants;
k_B is Boltzman's constant;
α_{Ti} is the thermo-diffusion coefficient;
T is the temperature, which, along with the diffusion coefficient of electrons or holes (D_i) is defined from the shock wave parameters:

$$T = T_0 + \frac{v^2}{2C_v}; \qquad v = \mu D; \tag{24}$$

$$D_i = \frac{1}{\mu_1}\left[D_{i0}(\mu_1 - \mu) + D_{i1}\mu\right]; \tag{25}$$

here $\mu = 1-\rho_0/\rho$ and $\mu_1 = 1-\rho_0/\rho_1$ describe the existent and the maximum degree of compression in the shock wave; ρ_0, ρ, ρ_1 are the initial, current and maximum material densities; D, v are the shock wave and the particle velocity, respectively; T_0 is the initial temperature. The input parameters D_{i1} and D_{i0} are entered into the model (see Eq. 25) as the diffusion coefficients in the compressed and uncompressed regions, respectively. The parameter D_{i0} is defined from the initial conductivity of the sample, whereas D_{i1} is varied for the best conformity with the experimental data. The degree of shock compression μ is presented in the running-wave form [21]:

$$\mu = \mu_1\left(1+\exp\left(\frac{4}{H}\left(x-(D-v_1)t\right)\right)\right)^{-1}; \tag{26}$$

$$H = \frac{16\eta}{\gamma_0 D\rho_0\mu_1 W}, \tag{27}$$

where v_1 is the maximum particle velocity;
H is the shock front width;
γ_0 is Grüneisen's coefficient;
η is the viscosity;
W is a function depending on the material parameters and the shock wave velocity [21] as

$$W = \frac{4}{\gamma_0\mu_1}\left\{1-\frac{1}{\rho_0 D^2}\left[\gamma_0 p_0 + 2G + \rho_0 C^2\,\frac{1-0.25\gamma_0\mu_1}{1-0.5S\mu_1}\right]\right\} - 1. \tag{28}$$

The non-stationary problem described by Eqs. (21–28) was solved numerically using in each time step the iteration procedure [23, 24], after which the total current density in the structure was calculated:

$$j = j_c + j_b = q\sum_{i=1}^{N} z_i J_i + \varepsilon\varepsilon_0 \frac{\partial E}{\partial t} \tag{29}$$

where j_c, j_b are the conduction and bias currents,

$E = -\nabla\varphi$ is the electric field.

Using the obtained value of the total current density j, the voltage drop U across the measuring resistor R can be estimated:

$$U = jSR, \tag{30}$$

where S is the sample's cross-section.

The U determination is the main objective of our calculations. It is this parameter that is called polarization or the EMF potential and is measured in the shock experiments.

Now, we will define some parameters needed for the calculations. Comparison of our Eq. (21) with Eqs. (1.2), (1.6) and (28') from [25] (Chap. 12) in the approximation of constant concentration $\nabla C_i = 0$ gives the thermo-diffusion coefficient as

$$\alpha_T = -\frac{\xi}{k_B T} + r + \frac{5}{2}, \tag{31}$$

where ξ is the chemical potential of the electron or hole;

r is the parameter defined from a scattering mechanism $r = 3/2$ for the ionized impurity scattering.

The mobilities of charge carriers are determined by the empirical formulae [13]:

$$\mu_n = 65 + \frac{1265}{1 + \left(\frac{n}{8.5 \cdot 10^{16}}\right)^{0.72}} \tag{32},$$

$$\mu_p = 44.7 + \frac{447}{1 + \left(\frac{p}{6.3 \cdot 10^{16}}\right)^{0.76}}, \tag{33}$$

where μ_n, μ_p are the electron and hole mobilities;

n, p are the concentrations of electrons and holes, respectively.

By these formulae, using the Einstein relationship $D_i = k_B T/q \cdot \mu_i$, the diffusion coefficients of electrons and holes were defined. The same formulae were employed for determination of the doping impurity concentration in experimental silicon samples with known conductivities based on the relationships $\sigma_n = qn\mu_n$ or $\sigma_p = qp\mu_p$.

4. COMPARISON WITH THE EXPERIMENTAL DATA

The authors of work [4] report the experimental data on the shock-induced polarization in silicon for two different amplitudes of the shock wave: 4 and 20 GPa. At 4 GPa there is only elastic wave, when the shock heating is not very strong

(a few degrees only) and practically does not change the initial concentration of charge carriers. Meanwhile, at 20 GPa, apart from the elastic wave, a plastic wave could occur, with an intense shock heating (several hundreds of degrees), resulting in strong ionization of the semiconductor with additional electrons and holes arising in the conductivity and valence zones, respectively. In the former case, the dominant mechanism of the shock-induced polarization is the separation of charge carriers and ionized impurity, whereas in the latter – the electron-hole separation owing to the difference both in the mobilities and in the thermo-diffusion coefficients. In the present work, the former case – as a simpler one – is considered. The case of the electron-hole separation will be treated in the work that follows.

The elastic wave parameters for silicon could be obtained using the data of work [26]. From Fig. 2 of that work it is seen that the elastic wave in the (111) direction is approximated by the straight line:

$$D = 9.36 + 0.96 v_1 \tag{34}$$

in the mass velocity range from 0 to 0.3 km/s. Using Eqs. (12), (13) and (20) the shock wave parameters could be chosen. Thus, from Eq. (13) the shear modulus G is determinable assuming that the end point of curve Eq. (34) at v_1 = 0.3 km/s corresponds to the pressure of 4 GPa. Parameter C could be found from Eq. (12) at $p_1 = 0$ and $v_1 = 0$ – the beginning point of curve Eq. (34) – under the supposition that at the zero pressure the shock wave velocity is equal to the sound speed. The remaining parameters, γ_0 and S, can be adjusted by matching Eq. (20) and the experimental curve (Eq. (34)). The results of estimation of the elastic shock wave parameters, along with some reference data, are presented in Table 1.

Table1

Material parameters used in the calculations

Parameters	Si	Units
Density, ρ_0	2.329	gm cm^{-3}
Specific heat, C_p	0.879	J gm^{-1} K^{-1}
Shear modulus, G	41	Gpa
Shear viscosity, ν	300	Poise
γ_0	0.85	
S	2.74	
C	7.236	km c^{-1}

First, we will consider the behaviour of low-doped samples of silicon under the shock load. This variant is simpler for modelling, since in this case the number of iterations made at each time step to obtain identical current values at any point of the sample is not too large. Besides, it would be instructive to know the value of current for low-doped samples at 4 GPa, since the experimental data in work [4] relate to 20 GPa only (see sample № 5 in Fig. 2 [4]).

Figure 1 displays the results of a testing calculation of shocked low-doped ($3.6 \cdot 10^{11}$ cm^{-3}) p-silicon at a shock wave amplitude of 4 GPa. The polarization signal is depicted as a voltage drop across a 100 ohm resistor with the current obtained numerically from Eqs. (21–23) and Eqs. (29, 30). The silicon sample contact

area was assumed to be 1 cm^2. These values of the resistance and the contact area (corresponds to the sample cross-section in our model) were employed in work [4]. In Fig. 1*a* the change in potential on the measuring resistor (a solid line) is shown for the time of shock wave propagation in the 4 GPa case, with the silicon parameters being as given in [4] for sample № 5. From the figure it is seen that at the beginning the potential rises sharply up to some value and, after a definite time, it rapidly falls to zero. The corresponding sections are associated with the shock wave front entering the sample and exiting from it. Between these sections the shock

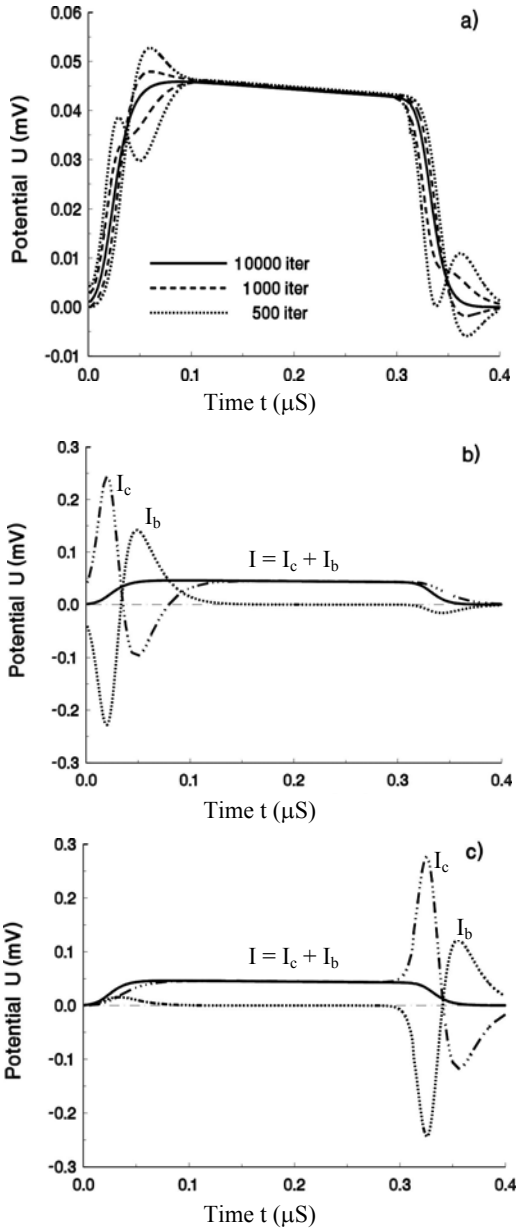

Fig 1. The total polarization current *I a*) and its components (conduction current I_c and bias current I_b) at the left *b*) and the right *c*) sample contacts of the low-doped ($3.6 \cdot 10^{11}$ cm^{-3}) *p*-silicon shocked at 4 GPa. All currents are shown as the potential drop on the resistor R = 100 ohm.

wave front is travelling through the sample, with the potential being almost constant. In Fig. 1*b,c* one can see the values of the total current and its components – the conduction current and the bias current on the left and right sample ends (contacts), respectively. The total current varies monotonically and practically in the same manner at both the ends, which proves the numerical calculations to be correct. The current components, in turn, change steeply and not equally on both the boundaries, especially when the shock wave front enters the sample or exits from it. Their sum, however, shows a monotonic behaviour, which evidences once again that the numerical calculations are true.

The conditions of the structural total current consistency can be derived only by performing the necessary iterations at each time step, which should be small enough. In the variant described above the time step was $\sim 10^{-10}$ s, with the number of iterations at each step being $\sim 5 \cdot 10^3$. This presents the necessary condition for correct calculation of the problem. Figure 1*a* shows (dashed lines) the total currents on the sample's boundaries that were obtained at a smaller number of iterations; this demonstrates the growth in error at calculations of the total current at the number of iterations decreasing.

The number of iterations should be raised if the doping level in silicon increases. When this level is $\sim 3.6 \cdot 10^{11}$, for calculation of a silicon structure several thousands of iterations are needed – a task that can be solved with modern PCs; at a doping level of $1 \cdot 10^{15}$-$1 \cdot 10^{18}$ the number of iterations rises tens and even hundreds of times. Therefore, more productive hardware is needed – such as GRID technologies, which have been employed for calculations of highly-doped structures in this work.

Despite quite a large value of the thermal diffusivity (α_T = 22 for $3.6 \cdot 10^{11}$ cm^{-3} from Eq. (31); this coefficient in semiconductors is the larger the lower the doping level) the structure with a doping level of $\sim 3.6 \cdot 10^{11}$ cm^{-3} exhibits very low values of the potential – several mV at the maximum (see Fig. 1*a*). This is three orders of magnitude lower than the potential values on the experimental polarization curves of work [4], where these values are in the range from 0.15 to 1.5 V; this means that to obtain such potential magnitudes one should raise either the level of silicon doping or the amplitude of the shock wave. Indeed, in work [4] the potentials of 0.15 V were obtained for *n*- and *p*-semiconductors with the doping level of $\sim 1 \cdot 10^{15}$ at 4 GPa, whereas at 20 GPa the potentials of 1.5 V were obtained both for a low-doped ($5 \cdot 10^{11}$) sample and for highly-doped ones ($\sim 1 \cdot 10^{15}$). Besides, the value and sign of the potential at 20 GPa do not depend on the doping level, which could be explained by a strong ionization of the semiconductor itself as a result of the shock heating. The potential at 4 GPa changes its sign for *n*- and *p*-types of semiconductor. This means that the charge carriers–ionized impurity separation model is valid at low pressures, which will be shown further by more specified calculations.

At the beginning we will consider the influence of conductivity increase or decrease behind the shock wave front upon the shape of the polarization signal. As is noted in Sect. 3, the conductivity changes have been modelled by variation in the diffusion coefficient of mobile charge carriers in the compression zone. In this connection it should be noted that the conductivity can also change as a result of the changed concentration of these carriers. However, to model the concentration

changes is a much more complicated task than to do this with their kinematical changes. Besides, in reasonable limits the modelling by both methods should give identical results, which will be employed further at the interpretation of the data obtained.

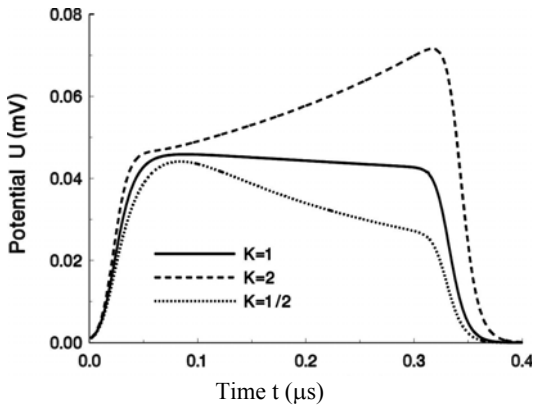

Fig. 2. Current-time characteristic of the low-doped ($3.6 \cdot 10^{11}$ cm^{-3}) *p*-silicon shocked at 4 GPa at different diffusion coefficients of holes ($K = D_1/D_0$) behind the shock wave front. As in Fig. 1, all currents are shown as the potential drop on the resistor R = 100 ohm.

Figure 2 by dashed lines shows the results of modelling the polarization currents in silicon at a double increase/decrease in the mobility of charge carriers behind the shock wave front. For comparison, by a solid line the results of modelling at constant mobility values are shown. In the figure it is seen that in the stationary section of the current-time characteristic (i.e. the shock wave front is travelling inside the sample) the current increases or decreases monotonically – depending on the increase or decrease in the mobility of charge carriers behind the front. Most probably, the currents will change in a similar manner at the charge carrier concentration changing in the same proportions. This – quite evident – supposition helps to interpret more completely the experimental results of work [4]. Thus, for example, from the mentioned work it follows that the polarization current increases monotonically at 20 GPa, which can be explained by an increase in the concentration of charge carriers under strong shock heating. Now, we will turn back to the polarization currents obtained at 4 Gpa.

Figure 3 shows the polarization currents obtained for *p*- and *n*-type silicon at 4 GPa (samples № 2 and № 6 in Ref. [4]) with the doping levels of $3.05 \cdot 10^{15}$ and $1.08 \cdot 10^{15}$ cm^{-3}, respectively. The calculations for such a high doping level were performed using Baltic-GRIG, taking about 48 hours for each variant ($6 \cdot 10^3$ time steps with $3 \cdot 10^5$ iterations in each step). The results of modelling are presented in the figure by solid lines, and the experimental data are shown by solid circles. The shock wave velocity at 4 GPa was taken 9.71 km/s (theoretical results), with an insignificant correction: 8.45 km/s for sample № 2 and 8.74 km/s for sample № 6, respectively. The shock wave front width was assumed to be equal to 0.4 mm for both the samples. The theoretically calculated shock heating was 45 degrees for 4 GPa, which, as was expected, practically did not change the carriers' concentration in the semiconductor. The resultant curves were obtained by fitting two

basic model parameters: the thermo-diffusion coefficient α_T and the ratio of diffusivities of charge carriers in compressed and non-compressed regions $K = D_1/D_0$. The best fitting with the experimental data has been obtained at $\alpha_T = 0.50$, $K = 0.15$ for sample № 2, and $\alpha_T = 0.79$, $K = 0.80$ for sample № 6. The values of thermo-diffusivities turned out to be somewhat below the theoretical estimates of these values for semiconductors (~12 from Eq. (31) for 10^{15} cm^{-3}), which could be attributed to the dynamical character of the process. The decrease in K is supposedly connected not with the decrease in the mobility of charge carriers in the compressed region but rather with their lower concentration owing to deionization of the doping impurity in semiconductor under pressure. As this takes place, the deionization in *p*-type silicon is much more intense than in *n*-type silicon (see Fig. 3).

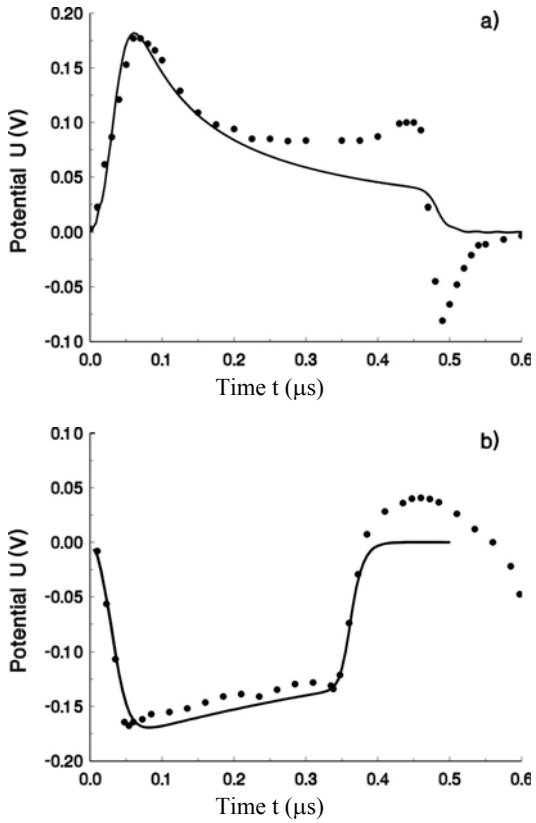

Fig 3. The potential drop on the resistor $R = 100$ ohm for
a) medium-doped ($3.05 \cdot 10^{15}$ cm^{-3}) *p*-silicon (sample № 2 in Ref. [4]) and
b) medium-doped ($1.08 \cdot 10^{15}$ cm^{-3}) *n*-silicon (sample № 6 in Ref. [4]) shocked at 4 GPa.
The thermo-diffusion coefficient and the ratio of mobilities are obtained
at $\alpha_T = 0.50$, $K = 0.15$ for sample № 2, and $\alpha_T = 0.79$, $K = 0.80$ for sample № 6.

The values of ionization degree and thermo-diffusivities can be refined in more perfect models. However, the very fact that the values of experimental polarization currents are obtained at lower thermo-diffusivities than this follows from the semiconductor theory counts in favour of the hypothesis about the thermo-diffusion as the dominant factor in arising of polarization currents in shocked semiconductors.

5. CONCLUSION

The straightforward method of modelling has been offered for the description of polarizing currents in shocked silicon at 4 GPa. The thermo-diffusion of the charge carriers in the temperature gradient of the shock wave front is calculated by the numerical method developed earlier for the electric characteristics of semiconductor devices. The comparison with the experimental data shows that the thermo-diffusion coefficient in semiconductors is large enough to explain the appearance of polarization current in the shocked silicon. Moreover, the impurity deionization behind the shock wave front follows from the analysis of the experimental polarization currents at 4 Gpa. These results show a good opportunity to derive the information on the physical phenomena in shocked materials from polarization currents.

ACKNOWLEDGMENT

The work was supported by the Latvian Council of Science (grant 06-1970) and by the European Union (FP6-2004-Infrastructures-6- contract No 026715 project "BalticGrid").

REFERENCES

1. Stepanov, A.V. (1933). *Zs. Phys.*, *81*, 560 (in Russian).
2. Linde, R.K., Murri, W.J., & Doran, D.G. (1966). *J. Appl. Phys.,37*, 2527.
3. Reyno1ds, C.E., & Seay, G.E. (1962). *J. Appl. Phys., 33*, 2234.
4. Mineev, V.N., Inanov, A.G., Lisicyn, Yu.V., Novickij, E.Z., & Tunjaev, Yu.N. (1970). *JETF, 59*, 1091 (in Russian).
5. Kanel, G.I., & Dremin, A.N. (1973). *Doklady AN, 211*, 1314 (in Russian).
6. Mineev, V.N., & Inanov, A.G. (1976). *Uspehi FN, 119*, 75 (in Russian).
7. Allison, F.E. (1965). *J. Appl. Phys.*, *36*, 2111.
8. Zel'dovich, Ya. B. (1967). *JETF, 53*, 237 (in Russian).
9. Inanov, A.G.., & Lisicyn, Yu.V., Novickij, E.Z. (1968). *JETF, 54*, 285 (in Russian).
10. Nesterenko, V.F(1974). *Fizika Gorenija i Vzryva, 10*, 752 (in Russian).
11. Migault, A., & Jacguesson, J. (1967). *C.R.Ac. Sci., B264***,** 507.
12. Mock, M. (1983). *Analysis of Mathematical Models of Semiconductor Devices.* Dublin: Boole Press.
13. Polsky, B. (1986). *Numerical Modelling of Semiconductor Devices.* Riga: Zinatne (in Russian).
14. Berman, F., Fox, G. & Hey, T. (eds) (2002). *Grid Computing – Making the Global Infrastructure a Reality*. New-York: John Wiley & Sons, Ltd ISBN: 0-470-85319-0.
15. Courant, R., & Friedrichs, K.O. (1999). *Supersonic Flow and Shock Waves.* New York, Heidelberg: Springer.
16. Nemat-Nasser, S., Okinaka, T. & Nesterenko, V., Liu, M. (1998). *Philosophical Magazine, A76,* 1151.
17. Wilkins, M.L. (1964). In: *Fundamental Methods in Hydrodynamics.3***.** London: Academic Press.
18. Samarsky, A.A., & Popov, Yu.P. (1985). *Difference Schemes of the Gas Dynamic.* Moscow: Nauka (in Russian).
19. Benson, D.J., & Conley, P. (1999). *Modeling Simul. Matter. Sci. Eng.,* (7), 333.
20. Slater J.C. (1939) *Introduction to Chemical Physics*. New York: McGraw-Hill, Chapt. 12–13.

21. Martuzans, B., Skryl, Yu., & Kuklja, M.M. (2002). Structure of the shock wave front in solids. *Latv. J. Phys. Tech. Sci.*, (3), 40–49.
22. Zeldovich, Ya.B. & Raizer, Yu.P. (2002). *Physics of shock waves and high-temperature hydrodynamic phenomena.* New York: Academic Press (eds: Hayes, W.D., & Probstein, R.F.).
23. Martuzans, B., & Skryl, Yu. (1998). *J. Chem. Soc. Faraday Trans*., *94*, 2411.
24. Skryl, Yu. (2000). *Phys. Chem. Chem. Phys*., (2), 2969.
25. Bonch-Bruevich V.L., Kalashnikov S.G. (1977) *Physic of Semiconductors.* Moscow: Nauka (in Russian).
26. Goto T., Sato T, Syono Y. (1982) *Jap. J. Appl. Phys. 21*(6), L369-L371.

LĀDIŅU PĀRNESES TRIECIENAM PAKĻAUTĀ SILICIJĀ SKAITLISKA MODELĒŠANA ZEMA SPIEDIENA GADĪJUMĀ

B. Martuzāns, J.. Skrils

K o p s a v i l k u m s

Izstrādāta skaitliska metode, lai modelētu elektronu un caurumu difūziju silicijā, kura notiek trieciena slodzes radītā temperatūras gradientā. Lai analizētu šo pārneses procesu, pilna lādiņu nesēju elektro-termodifūzijas vienādojumu sistēma tika risināta kopā ar Puasona vienādojumu. Skaitliskais risinājums tika iegūts ar diferenču metodes palīdzību, kura tika izstrādāta pusvadītāju iekārtām. Eksperimentālo rezultātu un skaitliskā risinājuma salīdzināšana uzrāda labu korelāciju, kas nozīmē, ka lādiņa nesēju termodifūzija trieciena viļņa frontē ir galvenais faktors, kurš atbild par polarizāciju triecienam pakļautā silicijā.

11.08.2008